

RPA calculations with Gaussian expansion method

H. Nakada^a, K. Mizuyama^b, M. Yamagami^c, M. Matsuo^d

^a *Department of Physics, Graduate School of Science, Chiba University,
Yayoi-cho 1-33, Inage, Chiba 263-8522, Japan*

^b *Department of Physics, University of Jyväskylä,
P. O. Box 35 (YFL), FI-40014, Jyväskylä, Finland*

^c *Department of Computer Science and Engineering, University of Aizu,
Aizu-Wakamatsu, Fukushima 965-8580, Japan*

^d *Department of Physics, Faculty of Science, Niigata University,
Niigata 950-2181, Japan*

November 14, 2018

Abstract

The Gaussian expansion method (GEM) is applied to calculations of the nuclear excitations in the random-phase approximation (RPA). We adopt the mass-independent basis-set that is successful in the mean-field calculations. The RPA results obtained by the GEM are compared with those obtained by several other available methods in Ca isotopes, by using a density-dependent contact interaction along with the Woods-Saxon single-particle states. It is confirmed that energies, transition strengths and widths of their distribution are described by the GEM with good precision, for the 1^- , 2^+ and 3^- collective states. The GEM is then applied to the self-consistent RPA calculations with the finite-range Gogny D1S interaction. The spurious center-of-mass motion is well separated from the physical states in the $E1$ response, and the energy-weighted sum rules for the isoscalar transitions are fulfilled reasonably well. Properties of low-energy transitions in ^{60}Ca are investigated in some detail.

PACS numbers: 21.60.Jz, 21.30.Fe, 21.10.Gv, 21.10.Pc

Keywords: RPA calculation; Gaussian expansion method; finite-range interaction; giant resonance.

1 Introduction

As atomic nuclei far off the β -stability exhibit exotic characters (*e.g.* nucleon halos [1] and new magic numbers [2]), excitation properties of unstable nuclei come under interest as well as their ground-state properties. The new features of unstable nuclei, such as the broad distribution of nucleons, the exotic shell structure and the coupling to the continuum, may give rise to new aspects of nuclear excitation. In theoretical studies of unstable nuclei, it is highly desired to handle those features efficiently. It is expected that ground-state properties of many nuclei can be investigated in the mean-field (MF) approximations, although correlation effects are not necessarily negligible. Among many efforts to develop new numerical methods to study structure of unstable nuclei, one of the authors (H.N.) proposed a method for MF calculations [3, 4, 5] that is based on the Gaussian expansion method (GEM) [6]. The GEM is adaptable to the broad distribution of nucleons, even with finite-range effective interactions including semi-realistic nucleon-nucleon (NN) interactions [7, 8]. The results of the MF calculations suggest that the continuum effects are properly taken into account by the GEM [4]. Moreover, we have found that the basis parameters in this method are insensitive to nuclide, and thereby even a single set of bases can be applied to wide mass range of nuclei [5]. Because of these advantages, it is of interest to use the GEM for describing excitations of unstable nuclei.

The random-phase approximation (RPA) provides us with a framework to treat one-particle-one-hole ($1p$ - $1h$) excitations of nuclei in a consistent manner with the MF description of the ground state. In this article we extensively apply the GEM to the RPA calculations. The strength functions of the spin-independent transitions are calculated in $^{40,48,60}\text{Ca}$. We first use the single-particle (s.p.) states in the Woods-Saxon potential and adopt a density-dependent contact interaction for the residual interaction. For this schematic Hamiltonian, reliable results are obtained by the continuum RPA [9]. We test the new method by comparing its results with the continuum RPA results, particularly for excitations of unstable nuclei. There have been many RPA calculations using the harmonic oscillator (HO) s.p. basis functions. It is popular as well to implement RPA calculations by assuming the box boundary for the s.p. states. The new method is also compared with these methods. The present method is then applied to fully self-consistent Hartree-Fock (HF) plus RPA calculations, by employing the finite-range Gogny interaction. We shall check whether the spurious center-of-mass (c.m.) excitation is well separated from the physical modes and how well the energy-weighted sum rules are satisfied. Properties of low-energy excitations in ^{60}Ca will also be discussed.

2 Methods of calculations

We shall consider the strength function,

$$S(\omega) = \sum_{\alpha} \delta(\omega - \omega_{\alpha}) \left| \langle \alpha | \mathcal{O} | 0 \rangle \right|^2, \quad (1)$$

where \mathcal{O} stands for the transition operator, $|0\rangle$ the ground state, ω_α the excitation energy of the state $|\alpha\rangle$. Below the particle-emission threshold we have discrete excited states. The sum over α in Eq. (1) is replaced by an energy integral for the continuum, if necessary. The response function is defined by

$$R(\omega) = \langle 0 | \frac{\mathcal{O}^\dagger \mathcal{O}}{\omega - H + i\eta} | 0 \rangle, \quad (2)$$

with η representing an infinitesimal positive number. $R(\omega)$ is related to $S(\omega)$ through

$$S(\omega) = -\frac{1}{\pi} \text{Im}[R(\omega)]. \quad (3)$$

By adding a finite imaginary number $i\gamma$ to the energy ω , we define

$$R_\gamma(\omega) = \langle 0 | \frac{\mathcal{O}^\dagger \mathcal{O}}{\omega - H + i\gamma} | 0 \rangle, \quad (4)$$

from which $S(\omega)$ is smeared out as

$$S_\gamma(\omega) = -\frac{1}{\pi} \text{Im}[R_\gamma(\omega)] = \frac{1}{\pi} \sum_\alpha \frac{\gamma}{(\omega - \omega_\alpha)^2 + \gamma^2} |\langle \alpha | \mathcal{O} | 0 \rangle|^2. \quad (5)$$

For the $1p$ - $1h$ excitations $S(\omega)$ (or $S_\gamma(\omega)$) is calculated from the transition amplitude $\langle \alpha | \mathcal{O} | 0 \rangle$ in the RPA, or from $R(\omega)$ (or $R_\gamma(\omega)$) in the linear response theory. It is well known that these two approaches are equivalent to each other [10]. We therefore do not distinguish them in this paper.

We here discuss several methods of calculating $S(\omega)$ or $S_\gamma(\omega)$ in the RPA. If we take a set of basis functions, the s.p. wave functions in the MF potential are given by superposing the bases. Solving the RPA equation that is represented by the s.p. states, we obtain the excited state $|\alpha\rangle$ (to be more precise, forward and backward amplitudes along with ω_α), from which $S(\omega)$ (or $S_\gamma(\omega)$) is calculated. In this type of methods, quality of the results is governed by the s.p. basis functions. In the RPA calculations of nuclei near the β -stability, it has been customary to employ the HO basis-set. However, it has been pointed out [3] that the HO set is impractical in handling the broad nucleon distribution and the coupling to the continuum, which could be important in unstable nuclei. In the present paper we propose a method using the GEM basis-set, which is comprised of multi-range Gaussian basis functions. Adaptable to the energy-dependent asymptotics of the s.p. wave functions including the oscillatory ones [4], the GEM basis-set is expected to describe the $1p$ - $1h$ excitations appropriately, up to the continuum effects.

It is also popular to obtain the s.p. wave functions by solving the MF equation in a discretized coordinate space. To keep the number of the s.p. states finite, one often confines the nucleons in a box or imposes a periodic boundary condition. In addition, truncation with respect to the s.p. energies is necessary in solving the RPA equation. While this method is feasible for contact NN interactions (or for local densities and

currents) such as the Skyrme interaction, it is not easy to be applied when a finite-range interaction is adopted¹.

In the linear response theory $R(\omega)$ (or $R_\gamma(\omega)$) is closely connected to the s.p. Green's function. The spectral representation, *i.e.* the expansion in terms of the s.p. states, may be employed for the s.p. Green's function [12]. It is also possible to take account of the exact form of the asymptotics of the s.p. Green's function at each ω , as was argued and carried out in Ref. [9]. This method is often called 'continuum RPA'. It is an additional advantage of the continuum RPA that we do not need truncation regarding the s.p. energies. The strength function $S(\omega)$ or $S_\gamma(\omega)$ is straightforwardly calculated from $R(\omega)$ or $R_\gamma(\omega)$, without constructing the excited state $|\alpha\rangle$ explicitly. We note that the continuum RPA was extended to the quasiparticle RPA in Refs. [13, 14]. Because it is implemented in a coordinate space, the continuum RPA is suitable for contact NN interactions.

There are other computational methods to implement the RPA calculations, although we do not treat them in this article. Recent developments include a method based on the mixed representation of the RPA equation [15], in which the unoccupied s.p. states are handled in a coordinate space [16]. The small amplitude limit of the time-dependent HF (TDHF) theory derives the RPA [10] as well. Methods to compute the linear responses via the TDHF have been explored [17]. One can carry out the TDHF calculations either by using s.p. bases or in a coordinate space. As a new approach based on the TDHF, the finite-amplitude method has been invented [18].

In all practical calculations in this paper, we assume that the ground states of the nuclei are well approximated by the spherical HF solutions. We shall compare results of several methods for $^{40,48,60}\text{Ca}$ in Sec. 3. In the following of this section we present computational details of the individual methods. We will focus on the method using the GEM in Sec. 4.

2.1 Gaussian expansion method

In the present paper we newly introduce a method of the RPA calculations using the Gaussian expansion method (GEM). In the GEM, both the ground and the excited states are represented by the s.p. basis functions having the following form:

$$\begin{aligned}\varphi_{\nu\ell jm}(\mathbf{r}) &= R_{\nu\ell j}(r) [Y^{(\ell)}(\hat{\mathbf{r}})\chi_\sigma]_m^{(j)}; \\ R_{\nu\ell j}(r) &= \mathcal{N}_{\nu\ell j} r^\ell \exp(-\nu r^2),\end{aligned}\tag{6}$$

where $Y^{(\ell)}(\hat{\mathbf{r}})$ expresses the spherical harmonics and χ_σ the spin wave function. We drop the isospin index without confusion. The range parameter of the Gaussian basis function ν , which is also used as an index of the bases, can be complex ($\nu = \nu_r + i\nu_i$) [6]. The

¹ It is mentioned that the Woods-Saxon basis functions, which are obtained in a coordinate space, have been used in Ref. [11] for a quasiparticle RPA calculation with the Gogny interaction.

constant $\mathcal{N}_{\nu\ell j}$ is determined by

$$\mathcal{N}_{\nu\ell j} = \frac{2^{\ell+\frac{7}{4}}}{\pi^{\frac{1}{4}}\sqrt{(2\ell+1)!!}} \nu_r^{\frac{2\ell+3}{4}}, \quad (7)$$

so as for $\langle\varphi_{\nu\ell jm}|\varphi_{\nu\ell jm}\rangle$ to be unity. We take the set comprised of all the bases of

$$\nu_r = \nu_0 b^{-2k}, \quad \begin{cases} \nu_i = 0 & (k = 0, 1, \dots, 5) \\ \frac{\nu_i}{\nu_r} = \pm \frac{\pi}{2} & (k = 0, 1, 2) \end{cases}, \quad (8)$$

with $\nu_0 = (2.40 \text{ fm})^{-2}$ and $b = 1.25$ (6 real functions and 6 complex functions), irrespectively of (ℓ, j) . With this basis-set we can describe ground states of many nuclei in a wide mass range from ^{16}O to ^{208}Pb [5]. We first solve a MF equation in the s.p. space spanned by the above bases. We note that, since the GEM bases are not orthogonal to one another, the MF equation leads to a generalized eigenvalue problem. The MF solution determines the s.p. states, by which we represent the RPA equation. We then solve the RPA equation, following Sec. 8.4.4 of Ref. [10].

2.2 Method of quasi-HO basis functions

The HO basis-set has been employed for many MF and RPA calculations so far. The radial part of the spherical HO basis function has the form of a Gaussian multiplied by the associated Laguerre's polynomial. As mentioned in Ref. [3], we can produce a basis-set that is equivalent to the HO set by extending the basis functions of Eq. (6); $R(r) \propto r^{\ell+2p} \exp(-\nu r^2)$ with an integer p , and ν restricted to a single real value. While the individual basis functions are not the same as the HO functions, the set comprised of them is equivalent to the HO basis-set of $\{L_p^{(\ell+\frac{1}{2})}(\sqrt{2\nu}r) r^\ell \exp(-\nu r^2); p = 0, 1, 2, \dots\}$ for each (ℓ, j) , where $L_p^{(\alpha)}(x)$ is the associated Laguerre's polynomial, as revealed if we apply the Gram-Schmidt orthogonalization. An analogous basis-set is produced from the basis functions of Eq. (6), by taking $\nu = \nu_0 b^{-2k}$ ($k = 0, 1, 2, \dots$) with real ν_0 and b close to unity. Indeed, if we take the $b = 1$ limit after orthogonalizing to the $k = 0$ basis $R_{\nu_0\ell j}(r) \propto r^\ell \exp(-\nu_0 r^2) = L_0^{(\ell+\frac{1}{2})}(\sqrt{2\nu_0}r) r^\ell \exp(-\nu_0 r^2)$, the $k = 1$ basis yields the HO basis of $L_1^{(\ell+\frac{1}{2})}(\sqrt{2\nu_0}r) r^\ell \exp(-\nu_0 r^2)$. It is easy to show that the basis proportional to $L_k^{(\ell+\frac{1}{2})}(\sqrt{2\nu_0}r) r^\ell \exp(-\nu_0 r^2)$ is produced by successive orthogonalization, and thereby we obtain a set equivalent to the HO basis-set. Obviously $2k + \ell$ corresponds to the number of the oscillator quanta N_{osc} in the HO bases. In practice, we adopt a set of the basis functions of Eq. (6) with $b = 1.05$ and ν_0 determined from $\omega_{\text{osc}} = 41.2 A^{-1/3} \text{ MeV}$ through $\nu_0 = \sqrt{2/M\omega_{\text{osc}}}$. This set will be called 'quasi-HO' basis-set hereafter. The space spanned by the bases satisfying $2k + \ell \leq 11$ is taken in the calculations in Sec. 3. With this basis-set we solve the MF and RPA equations in the same manner as in Subsec. 2.1.

2.3 Coordinate-space method with box boundary

If the MF is local, it is not difficult to solve the MF equation in a coordinate space. Because we assume the spherical symmetry, it is sufficient to consider one-dimensional coordinate space of the radial variable. This radial coordinate is discretized by a mesh whose size is denoted by h . We impose a box boundary condition that the s.p. wave functions should vanish at r_{\max} . The MF equation is solved in the coordinate space thus determined. In Sec. 3 we adopt $h = 0.2$ fm and $r_{\max} = 20$ fm, confirming the convergence in the MF calculations.

The RPA Hamiltonian is represented by the s.p. states obtained in the MF calculation, by cutting off the unperturbed excitation energy at $\Delta\varepsilon_{\text{cut}}$. In practical calculations in Sec. 3, we do not solve the eigenvalue problem defined by the RPA equation, but we instead compute $R_\gamma(\omega)$ by solving the Bethe-Salpeter equation in the spectral representation [12] (using the s.p. states and $\Delta\varepsilon_{\text{cut}}$). The strength function $S_\gamma(\omega)$ is then obtained via Eq. (3) (or (5)). For certain transition modes the RPA results are slow to converge for increasing $\Delta\varepsilon_{\text{cut}}$ [19]. We have confirmed that $S_\gamma(\omega)$ at $\omega < 30$ MeV has no visible difference between $\Delta\varepsilon_{\text{cut}} = 150$ MeV and 200 MeV for all the modes under consideration.

2.4 Continuum RPA

In the continuum RPA [9], the strength function is calculated from the response function. However, the response function is constructed from the s.p. orbits of holes and the s.p. Green's function for the excited particles, unlike the spectral representation. The asymptotic form of the s.p. Green's function at large r , which depends on ω , is known for each partial wave. For each ω , the inner part of the s.p. Green's function is continued to the proper asymptotic form at a sufficiently large r . Hence the calculation is free both from the boundary at r_{\max} and from the energy cut-off like $\Delta\varepsilon_{\text{cut}}$. For a relatively simple interaction as used in Sec. 3, we can obtain 'exact' transition strength functions (which are exact within the RPA), as long as the convergence with respect to h is reached. In the continuum RPA calculations in Sec. 3, we follow the method shown in Ref. [13], except that we do not need integration in the complex energy plane because we do not have pair correlations in the ground state. The mesh size h is taken to be 0.2 fm as in the box-boundary calculation, for which the convergence has been confirmed.

Whereas the continuum RPA calculations are implemented with specifying ω , it is not easy to pinpoint the excitation energies of the discrete states. To avoid missing the discrete levels, we calculate $S_\gamma(\omega)$ rather than $S(\omega)$, taking $\gamma = 0.2$ MeV. The excitation energy and the transition strength of each discrete state is extracted by fitting $S_\gamma(\omega)$ around the peak to a Lorentzian. Correspondingly, we compute $S_\gamma(\omega)$ with $\gamma = 0.2$ MeV in the other methods, by using the imaginary energy $\omega + i\gamma$ in the method of Subsec. 2.3 and by smearing out $S(\omega)$ in those of Subsecs. 2.1 and 2.2.

3 Comparison of methods for contact force

In this section numerical results of the four methods explained in the preceding section 2.1–2.4 are compared. For this purpose, we take the nuclear MF of the Woods-Saxon potential to which the Coulomb potential is added, as adopted in Ref. [9]:

$$U(\mathbf{r}) = \left(1 - 0.67 \frac{N - Z}{A} \tau_z\right) \left(U_0 f(r) + U_{\ell s} \boldsymbol{\ell} \cdot \mathbf{s} \frac{1}{r} \frac{d}{dr} f(r)\right) + \frac{1}{2} (1 - \tau_z) U_C(r), \quad (9)$$

where $f(r) = 1/[1 + \exp((r - R)/a)]$, $U_0 = -58 \text{ MeV}$, $U_{\ell s} = 30 \text{ MeV fm}^2$, $R = 1.20(A - 1)^{1/3} \text{ fm}$, $a = 0.65 \text{ fm}$, $\tau_z = +1$ (-1) for a neutron (a proton), and $U_C(r)$ is the Coulomb potential produced by the uniform charge distribution of $(Z - 1)$ protons in the sphere of radius R . For the residual interaction, we assume the density-dependent contact force as

$$\hat{v}_{\text{res}} = f \left[t_0 (1 + x_0 P_\sigma) \delta(\mathbf{r}_1 - \mathbf{r}_2) + \frac{1}{6} t_3 (1 + x_3 P_\sigma) \rho(\mathbf{r}_1) \delta(\mathbf{r}_1 - \mathbf{r}_2) \right], \quad (10)$$

with $t_0 = -1100 \text{ MeV fm}^3$, $x_0 = 0.5$, $t_3 = 16000 \text{ MeV fm}^6$ and $x_3 = 1$ [9]. $\rho(\mathbf{r})$ denotes the nucleon density, and P_σ the spin exchange operator. It will be stated below how to fix the overall factor f . The spin densities arising from \hat{v}_{res} are ignored for the sake of simplicity.

We shall consider transitions carried by the one-body operator,

$$\mathcal{O}^{(\lambda, \tau)} = \sum_i r_i^\lambda Y^{(\lambda)}(\hat{\mathbf{r}}_i) \begin{cases} 1 & (\text{for } \tau = 0) \\ \tau_z & (\text{for } \tau = 1) \end{cases}, \quad (11)$$

with $\lambda = 1, 2, 3$, where i denotes the index of nucleons, for the ^{40}Ca , ^{48}Ca and ^{60}Ca nuclei. The $(\lambda = 1, \tau = 0)$ mode corresponds to the spurious c.m. motion. Subtracting its contribution, we obtain a modified operator for the $(\lambda = 1, \tau = 1)$ mode,

$$\tilde{\mathcal{O}}^{(\lambda=1, \tau=1)} = \frac{2Z}{A} \sum_{i \in n} r_i Y^{(1)}(\hat{\mathbf{r}}_i) - \frac{2N}{A} \sum_{i \in p} r_i Y^{(1)}(\hat{\mathbf{r}}_i), \quad (12)$$

which is proportional to the $E1$ operator with the c.m. correction. The expression $i \in n$ ($i \in p$) indicates that the sum includes the i -th nucleon if it is a neutron (proton). The strength functions $S^{(\lambda, \tau)}$ and $S_\gamma^{(\lambda, \tau)}$ are defined by substituting $\mathcal{O}^{(\lambda, \tau)}$ in Eqs. (1,5). For the $(\lambda = 1, \tau = 1)$ mode we can define $\tilde{S}^{(\lambda=1, \tau=1)}$ and $\tilde{S}_\gamma^{(\lambda=1, \tau=1)}$ from $\tilde{\mathcal{O}}^{(\lambda=1, \tau=1)}$. The renormalization parameter f in Eq. (10) is determined so that the spurious c.m. state should have zero excitation energy [9], for individual cases. We tabulate the f values thus determined in Table 1. Although there is no consistency between the MF and the residual interaction, this set of the MF potential and the interaction is suitable for assessing the numerical methods.

In Figs. 1–5 we display the strength functions $S_\gamma^{(\lambda, \tau)}(\omega)$. For the calculations assuming the box boundary shown in Subsec. 2.3, we take $\Delta \varepsilon_{\text{cut}} = 50 \text{ MeV}$, whose results are not qualitatively different from those of $\Delta \varepsilon_{\text{cut}} = 200 \text{ MeV}$.

If we estimate from the s.p. energies, the particle threshold lies at $\omega = 8.7 \text{ MeV}$ for ^{40}Ca and ^{48}Ca , while at 3.4 MeV for ^{60}Ca . In all the three nuclei we find $\lambda = 3$ peaks

Table 1: Adopted values of f , the renormalization factor of the residual interaction. The label ‘Cont.’ (‘Box’) indicates the case of the continuum RPA (the box-boundary method).

nuclide	Cont.	Box	quasi-HO	GEM
^{40}Ca	0.691	0.785	0.715	0.700
^{48}Ca	0.711	0.808	0.750	0.720
^{60}Ca	0.758	0.842	0.796	0.764

at low ω that correspond to discrete states. For ^{48}Ca we also find low-lying discrete 2^+ states because of the shell structure. Although the 8.86 MeV state in the $\lambda = 3$ excitation of ^{48}Ca is located just above the neutron threshold, it behaves like a discrete state. For these discrete states we list the excitation energies ω_α and the transition strengths

$$B_\alpha^{(\lambda,\tau)} = \left| \langle \alpha | \mathcal{O}^{(\lambda,\tau)} | 0 \rangle \right|^2 = \int_{\omega_\alpha - \eta}^{\omega_\alpha + \eta} S^{(\lambda,\tau)}(\omega) d\omega, \quad (13)$$

in Table 2. The low-lying 3^- state is highly collective in any of the three nuclei. For this state the convergence for $\Delta\varepsilon_{\text{cut}}$ is quite slow in the calculation under the box boundary condition, and we show the results with $\Delta\varepsilon_{\text{cut}} = 200$ MeV in Table 2. Note that the $S_\gamma^{(\lambda,\tau)}(\omega)$ graphs in Figs. 4 and 5 do not much change even if we take $\Delta\varepsilon_{\text{cut}} = 200$ MeV.

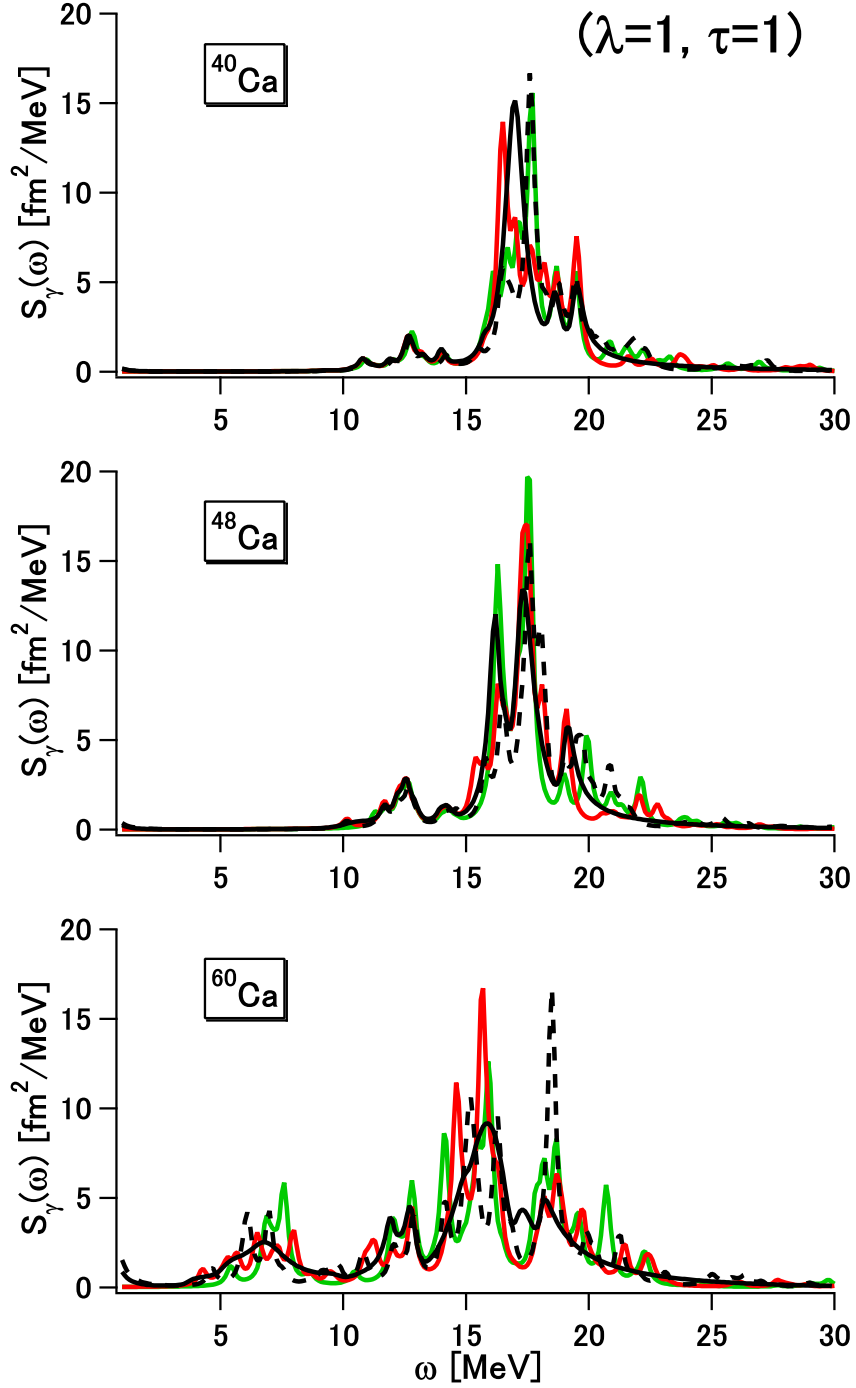


Figure 1: $\tilde{S}_{\gamma}^{(\lambda=1, \tau=1)}(\omega)$ in $^{40,48,60}\text{Ca}$, by the RPA calculations using the mean field of Eq. (9) and the residual interaction of Eq. (10). Results of the continuum RPA, the box-boundary method, the method employing the quasi-HO bases and the GEM are represented by the black solid, the black dashed, the green solid and the red solid lines, respectively. We take $\gamma = 0.2 \text{ MeV}$ for all the calculations.

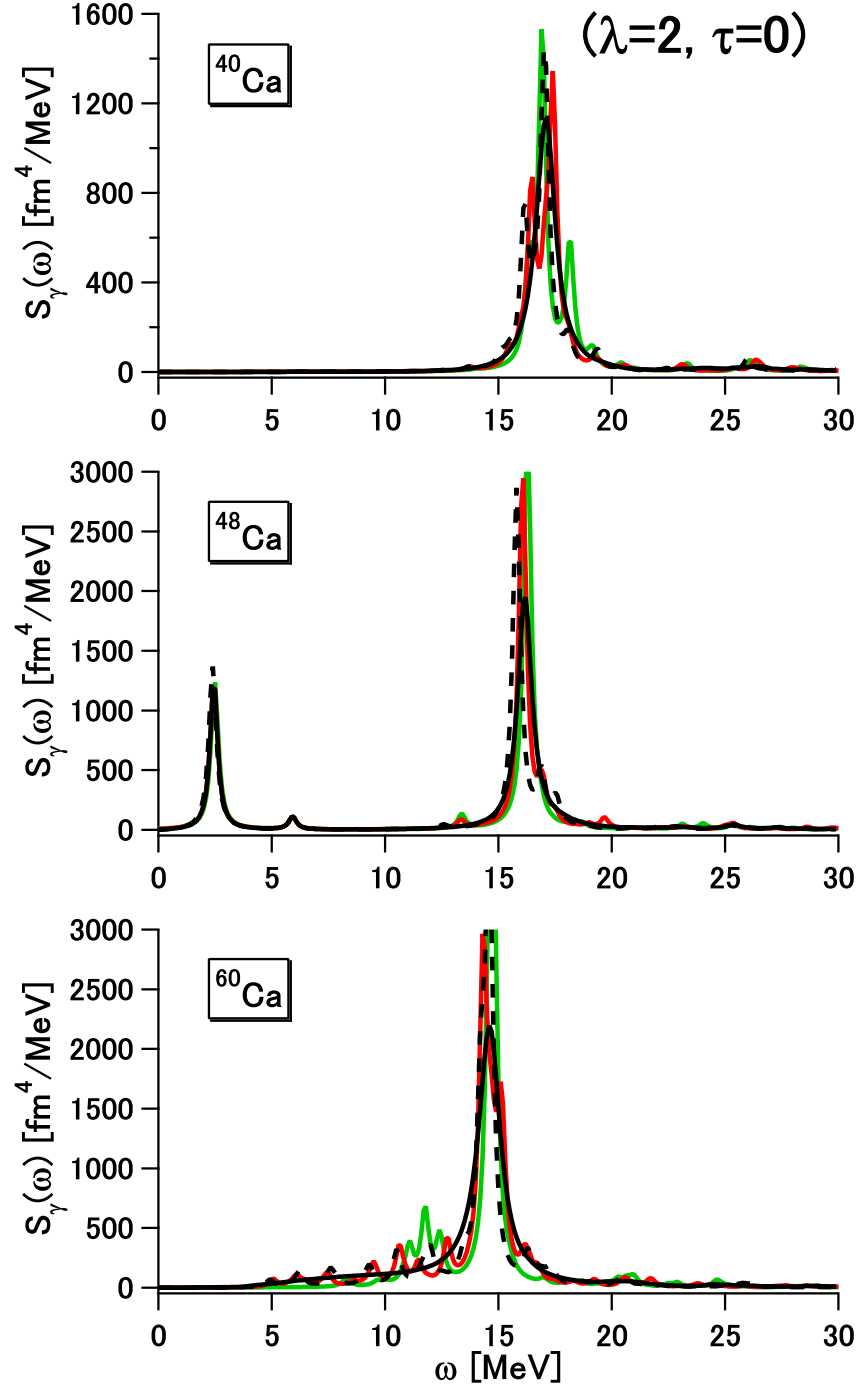


Figure 2: $S_\gamma^{(\lambda=2, \tau=0)}(\omega)$ in $^{40,48,60}\text{Ca}$. See Fig. 1 for conventions.

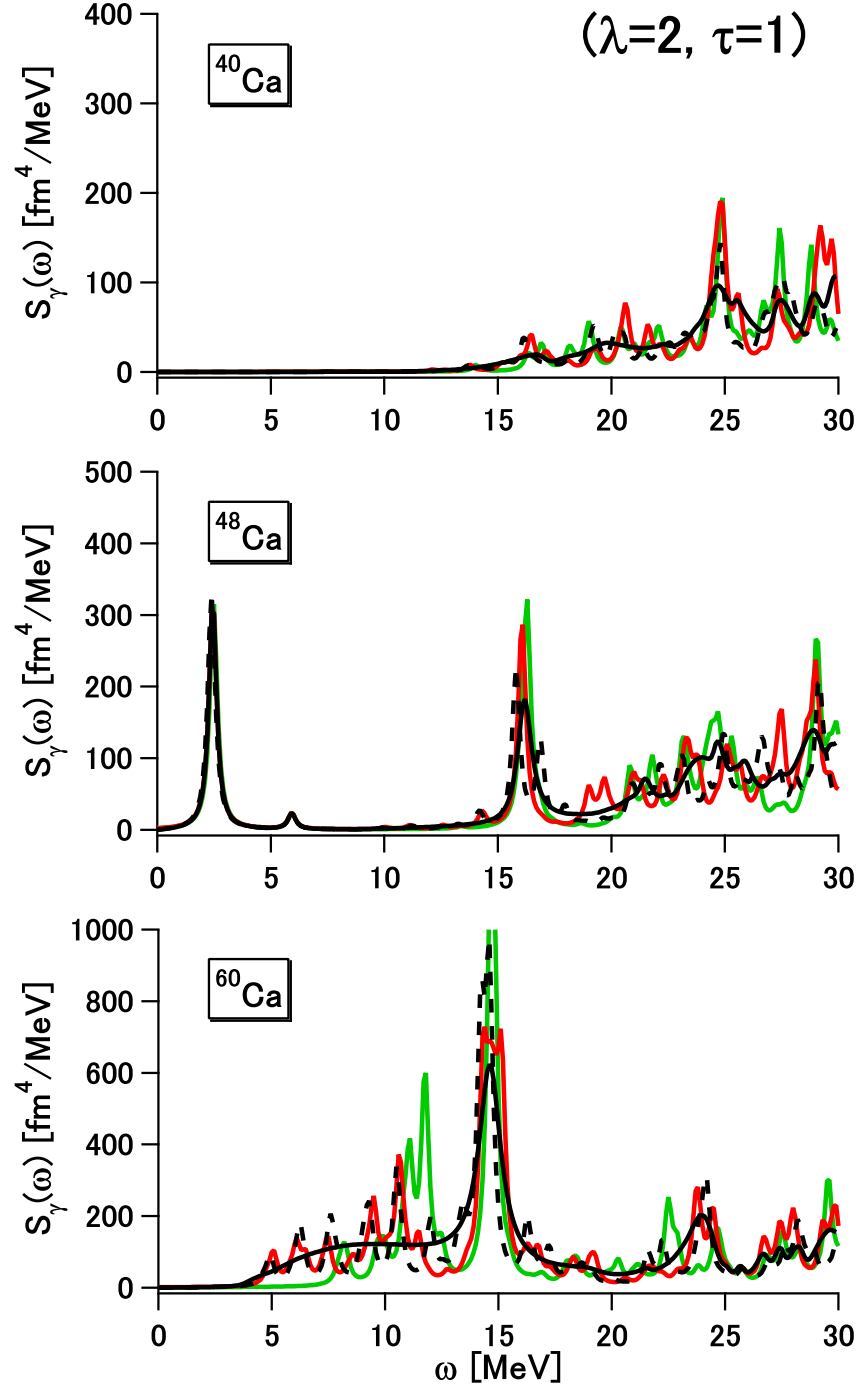


Figure 3: $S_\gamma^{(\lambda=2, \tau=1)}(\omega)$ in $^{40,48,60}\text{Ca}$. See Fig. 1 for conventions.

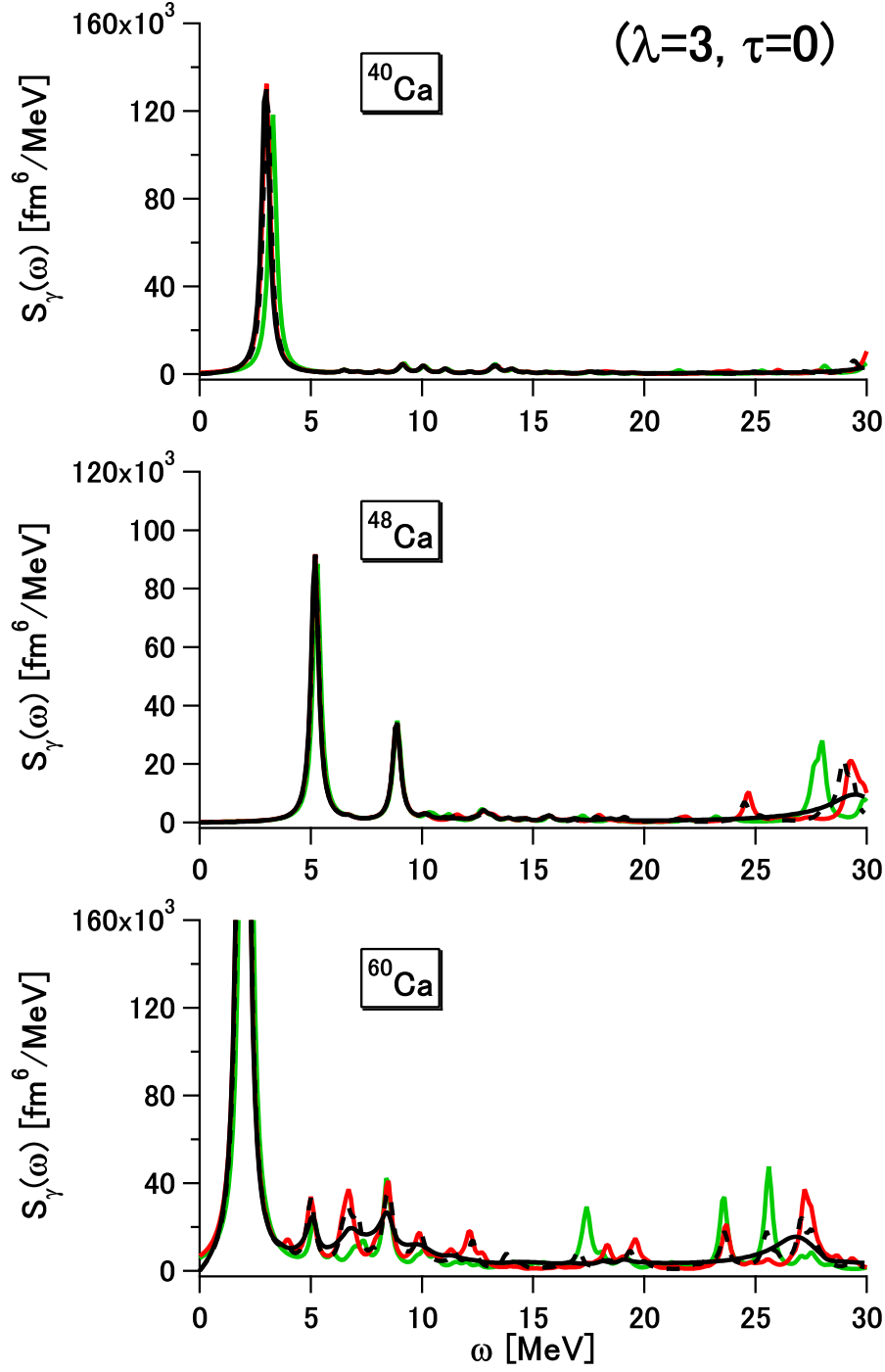


Figure 4: $S_\gamma^{(\lambda=3, \tau=0)}(\omega)$ in $^{40,48,60}\text{Ca}$. See Fig. 1 for conventions.

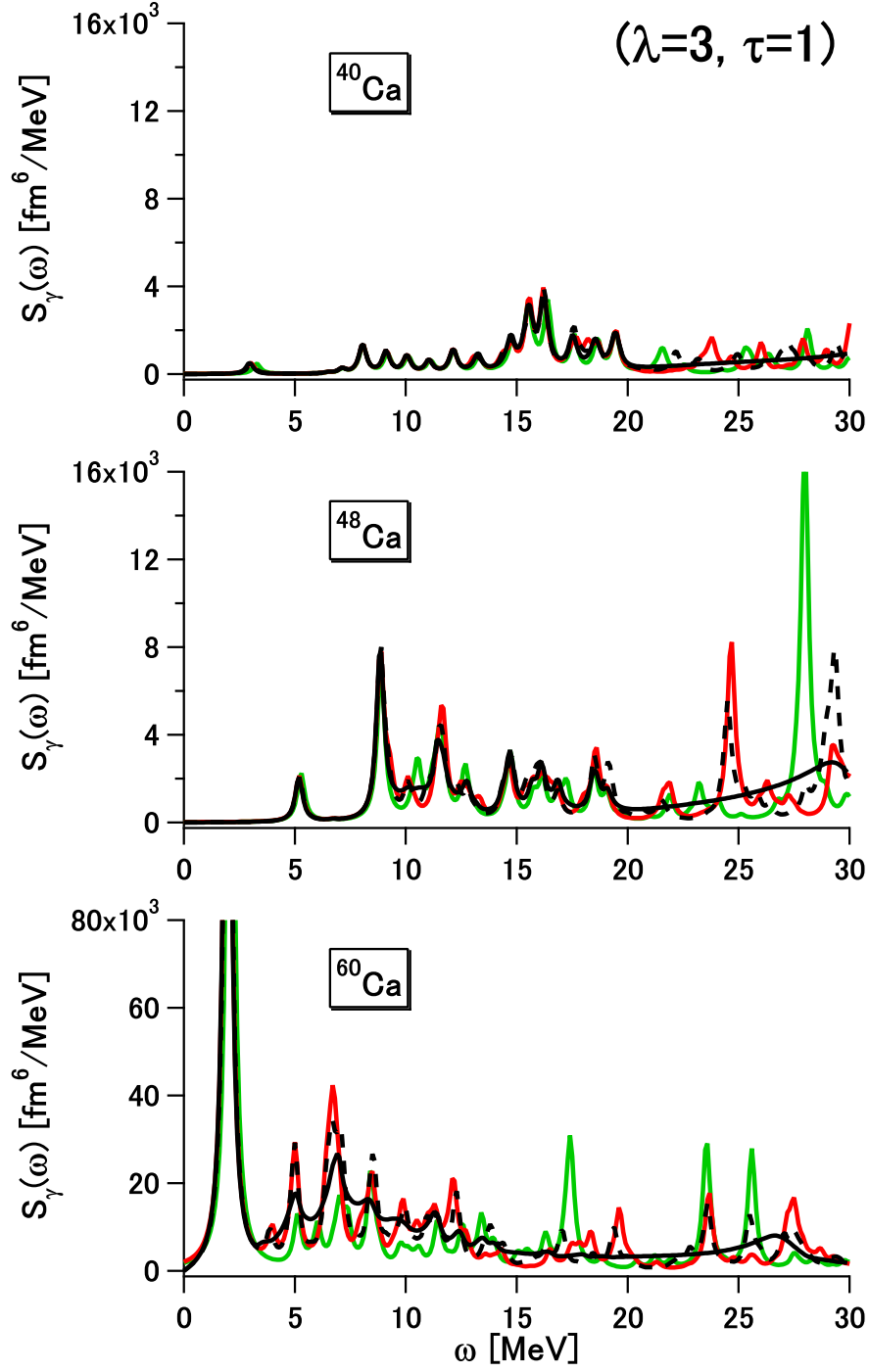


Figure 5: $S_\gamma^{(\lambda=3, \tau=1)}(\omega)$ in $^{40,48,60}\text{Ca}$. See Fig. 1 for conventions.

Table 2: Excitation energy ω_α (MeV) and transition strength $B_\alpha^{(\lambda,\tau)}$ ($\text{fm}^{2\lambda}$) for each discrete state, obtained by the RPA calculations employing the mean field of Eq. (9) and the residual interaction of Eq. (10). Results of the continuum RPA, the box-boundary method, the method using the quasi-HO bases and the GEM are compared.

nuclide			Cont.		Box		quasi-HO		GEM	
	λ	τ	ω_α	$B_\alpha^{(\lambda,\tau)}$	ω_α	$B_\alpha^{(\lambda,\tau)}$	ω_α	$B_\alpha^{(\lambda,\tau)}$	ω_α	$B_\alpha^{(\lambda,\tau)}$
^{40}Ca	3	0	2.96	8.49×10^4	3.04	8.20×10^4	3.28	7.51×10^4	3.00	8.32×10^4
		1		3.29×10^2		3.25×10^2		2.97×10^2		3.20×10^2
^{48}Ca	2	0	2.45	7.88×10^2	2.45	7.87×10^2	2.49	7.78×10^2	2.45	7.89×10^2
		1		2.03×10^2		2.02×10^2		1.99×10^2		2.03×10^2
	2	0	5.92	7.38×10^1	5.92	7.38×10^1	5.93	6.68×10^1	5.92	6.85×10^1
		1		1.57×10^1		1.56×10^1		1.42×10^1		1.43×10^1
	3	0	5.18	5.82×10^4	5.20	5.77×10^4	5.27	5.66×10^4	5.19	5.77×10^4
		1		1.33×10^3		1.36×10^3		1.41×10^3		1.31×10^3
^{60}Ca	3	0	8.86	2.22×10^4	8.86	2.24×10^4	8.89	2.17×10^4	8.86	2.17×10^4
		1		5.35×10^3		5.48×10^3		4.68×10^3		4.81×10^3
	3	0	1.96	4.07×10^5	1.98	4.02×10^5	2.09	3.91×10^5	1.97	4.06×10^5
		1		1.15×10^5		1.15×10^5		1.17×10^5		1.15×10^5

By comparing with the results of the continuum RPA, we find that the maximum deviation of ω_α is 0.08, 0.32 and 0.04 MeV in the box-boundary, the quasi-HO and the GEM results, respectively. The relative error of $B_\alpha^{(\lambda,\tau)}$ is 3% in the box-boundary, 13% in the quasi-HO and 10% in the GEM results, at maximum. Thus, as long as the discrete states are concerned, the GEM provides precision of ~ 0.05 MeV for ω_α and $\sim 10\%$ for B_α . The precision of the GEM for ω_α is slightly better than that of the box-boundary calculations, and substantially better than that of the calculations using the quasi-HO bases. Although the precision might look worse than the box-boundary method for B_α , the strong transitions are described with good precision. It is noticed that the quasi-HO basis-set gives rise to sizable errors for the lowest-lying 3^- states.

Above the particle-emission threshold, the continuum RPA gives smooth $S(\omega)$ (*i.e.* the $\gamma \rightarrow 0$ limit of $S_\gamma(\omega)$), whereas in the other methods $S(\omega)$ is still represented by a sum of the delta functions. In Figs. 1–5 the strength functions are smoothed by the width parameter $\gamma (= 0.2 \text{ MeV})$. It is a clear advantage of the continuum RPA that the smooth behavior of $S(\omega)$ in the continuum is automatically taken into account, and could be important in investigating certain aspects of transitions, *e.g.* the soft dipole responses near the threshold [13, 20]. However, at higher ω the strength functions should further be smeared due to coupling to the $2p$ - $2h$ degrees of freedom, which is not incorporated in the usual RPA. Therefore gross properties of the strength distribution will be more important than its fine structure, when we view the RPA results. In Table 3, we tabulate the transition strength, the average energy and its standard deviation in an energy domain $D = \{\omega; \omega_D^{\min} < \omega < \omega_D^{\max}\}$;

$$\begin{aligned} B_D^{(\lambda,\tau)} &= \int_D S_\gamma^{(\lambda,\tau)}(\omega) d\omega, \\ \bar{\omega}_D^{(\lambda,\tau)} &= \int_D \omega S_\gamma^{(\lambda,\tau)}(\omega) d\omega / B_D^{(\lambda,\tau)}, \\ \sigma_D^{(\lambda,\tau)} &= \left[\int_D (\omega - \bar{E}_x)^2 S_\gamma^{(\lambda,\tau)}(\omega) d\omega / B_D^{(\lambda,\tau)} \right]^{1/2}. \end{aligned} \quad (14)$$

The domain D is chosen so as to cover the broad resonance-like structure of $S^{(\lambda,\tau)}(\omega)$. For the $(\lambda = 1, \tau = 1)$ mode, we use $\tilde{S}_\gamma^{(\lambda=1,\tau=1)}(\omega)$ instead of $S_\gamma^{(\lambda=1,\tau=1)}(\omega)$ as before.

Table 3: Comparison of $B_D^{(\lambda,\tau)}$ ($\text{fm}^{2\lambda}$), $\bar{\omega}_D^{(\lambda,\tau)}$ (MeV) and $\sigma_D^{(\lambda,\tau)}$ (MeV) in a certain energy range D , which is specified by ω_D^{\min} and ω_D^{\max} (MeV).

nuclide				Cont.			Box			quasi-HO			GEM		
	λ	τ	D	$B_D^{(\lambda,\tau)}$	$\bar{\omega}_D^{(\lambda,\tau)}$	$\sigma_D^{(\lambda,\tau)}$	$B_D^{(\lambda,\tau)}$	$\bar{\omega}_D^{(\lambda,\tau)}$	$\sigma_D^{(\lambda,\tau)}$	$B_D^{(\lambda,\tau)}$	$\bar{\omega}_D^{(\lambda,\tau)}$	$\sigma_D^{(\lambda,\tau)}$	$B_D^{(\lambda,\tau)}$	$\bar{\omega}_D^{(\lambda,\tau)}$	$\sigma_D^{(\lambda,\tau)}$
^{40}Ca	1	1	10.0 – 25.0	7.78×10^0	17.35	2.38	7.44×10^0	17.85	2.40	7.72×10^0	17.54	2.38	7.82×10^0	17.43	2.43
	2	0	12.0 – 22.0	1.66×10^3	17.12	1.10	1.67×10^3	16.88	1.14	1.63×10^3	17.23	1.12	1.66×10^3	17.09	1.10
		1	12.0 – 30.0	6.61×10^2	24.49	3.98	5.95×10^2	24.29	3.99	6.43×10^2	24.65	3.72	6.88×10^2	24.73	4.06
^{48}Ca	1	1	10.0 – 25.0	9.33×10^0	17.06	2.45	8.92×10^0	17.61	2.47	9.29×10^0	17.37	2.56	9.40×10^0	17.15	2.49
	2	0	12.0 – 22.0	2.29×10^3	16.32	1.16	2.28×10^3	16.13	1.13	2.26×10^3	16.30	1.07	2.29×10^3	16.30	1.19
		1	12.0 – 30.0	1.08×10^3	23.36	4.67	9.90×10^2	23.09	4.80	1.04×10^3	23.40	4.70	1.09×10^3	23.43	4.70
^{60}Ca	3	1	10.0 – 22.0	1.71×10^4	15.08	3.22	1.62×10^4	15.30	3.25	1.55×10^4	14.65	3.20	1.70×10^4	15.11	3.27
	1	1	2.0 – 10.0	2.11×10^0	6.75	1.54	1.90×10^0	6.71	1.55	1.84×10^0	7.17	1.07	2.09×10^0	6.81	1.49
			10.0 – 25.0	1.04×10^1	16.24	2.86	1.01×10^1	16.74	2.95	1.04×10^1	16.54	2.89	1.04×10^1	16.31	2.84
15	2	0	10.0 – 20.0	4.09×10^3	14.48	1.52	4.09×10^3	14.38	1.53	4.18×10^3	14.24	1.56	4.09×10^3	14.42	1.54
		1	3.0 – 12.8	8.85×10^2	9.06	2.32	8.72×10^2	8.98	2.25	8.78×10^2	10.80	1.43	8.92×10^2	8.98	2.16
			12.8 – 20.0	1.28×10^3	15.16	1.54	1.31×10^3	15.01	1.47	1.11×10^3	15.25	1.44	1.30×10^3	15.30	1.43
	3	0	3.5 – 15.0	1.30×10^5	7.97	2.72	1.31×10^5	7.91	2.73	8.66×10^4	7.89	2.66	1.34×10^5	7.94	2.67
			15.0 – 30.0	8.49×10^4	23.78	4.00	8.35×10^4	23.74	3.91	9.84×10^4	22.49	3.85	8.91×10^4	24.09	3.95
	3	1	3.5 – 15.0	1.31×10^5	8.47	2.86	1.28×10^5	8.48	2.89	8.15×10^4	9.08	2.98	1.32×10^5	8.43	2.80
			15.0 – 30.0	6.13×10^4	22.81	4.15	6.13×10^4	22.88	4.12	7.73×10^4	21.73	4.11	6.40×10^4	23.07	4.19

In Table 3 we find that the errors in the GEM results are 0.3 MeV for $\bar{\omega}_D^{(\lambda,\tau)}$, 5% for $B_D^{(\lambda,\tau)}$ and 0.2 MeV for $\sigma_D^{(\lambda,\tau)}$ at maximum, which are compared to 0.5 MeV (1.1 MeV), 10% (30%) and 0.1 MeV (0.9 MeV) in the box-boundary (the quasi-HO) results. We thus confirm that the GEM reproduces distribution of the transition strengths with good precision up to $\sigma_D^{(\lambda,\tau)}$, from stable to drip-line nuclei.

In Figs. 1–5, we view considerable transition strengths at low ω in ^{60}Ca , which arise due to the loosely bound neutrons. Similar results have been reported in the continuum RPA calculations with the Skyrme interaction [21, 22, 23]. Whereas such low-lying transition strengths in drip-line nuclei will be investigated further in a forthcoming paper, we here argue dependence of the results on the computational methods. In comparison to the results obtained with the other methods, notable deviation is found in the quasi-HO results for the strengths at $\omega \lesssim 10$ MeV. This is because the quasi-HO basis functions are not suitable for describing loosely bound nucleons which may have broad spatial distribution. To clarify this point, we consider the transition density defined by

$$r^2\rho_{\text{tr},\tau_z}^{(\lambda)}(r;\alpha) = \langle \alpha | \sum_{i \in \tau_z} \delta(r - r_i) r_i^\lambda Y^{(\lambda)}(\hat{\mathbf{r}}_i) | 0 \rangle \quad (\tau_z = p, n). \quad (15)$$

In Fig. 6, the neutron transition densities are depicted for the low-energy $\lambda = 3$ modes of ^{60}Ca . We present the transition densities at two prominent peaks in $5 < \omega < 7.5$ MeV obtained in the GEM and the quasi-HO calculations. For comparison, the densities in the continuum RPA are also displayed, whose renormalization factors (C in Eq. (17) of Ref. [20]) are determined so that the densities should be comparable to their counterparts in the GEM and the quasi-HO results.

It is found that the transition densities depend primarily on the s.p. bases, *i.e.* the GEM or the quasi-HO, rather than on the excitation energies of the states. These low-energy transitions are dominated by excitation of a neutron from the pf -shell to the continuum. The rapid decrease of $r^2\rho_{\text{tr},n}^{(\lambda=3)}(r;\alpha)$ at $r \approx 9$ fm in the quasi-HO results is attributed to limitation of the basis functions mentioned above. It does not seem easy to describe such transitions properly, even if we increase the number of the quasi-HO basis functions. On the contrary, the GEM gives broad distribution of $r^2\rho_{\text{tr},n}^{(\lambda=3)}(r;\alpha)$, in fair agreement with the corresponding transition densities in the continuum RPA. This implies that by the GEM we can take into account the effects of coupling to the continuum sufficiently. We here comment that $r^2\rho_{\text{tr},n}^{(\lambda=3)}(r;\alpha)$ obtained with the box-boundary method is also close to that of the continuum RPA in this energy region.

We have thus established that the method using the A -independent GEM basis functions of Eq. (8) is capable of describing the excitation energies, the transition strengths and the widths of their distribution with good precision, including nuclei in vicinity of the drip line, within the RPA framework. This method gives precision comparable to the method assuming the box boundary, and substantially better than the method using the quasi-HO basis functions for nuclei near the neutron drip line. The present method based on the GEM cannot reproduce the smooth energy dependence of the transition strengths in the continuum region. This is a defect if compared to the continuum RPA method. On the other hand, the GEM has an advantage in adaptability to finite-range interactions.

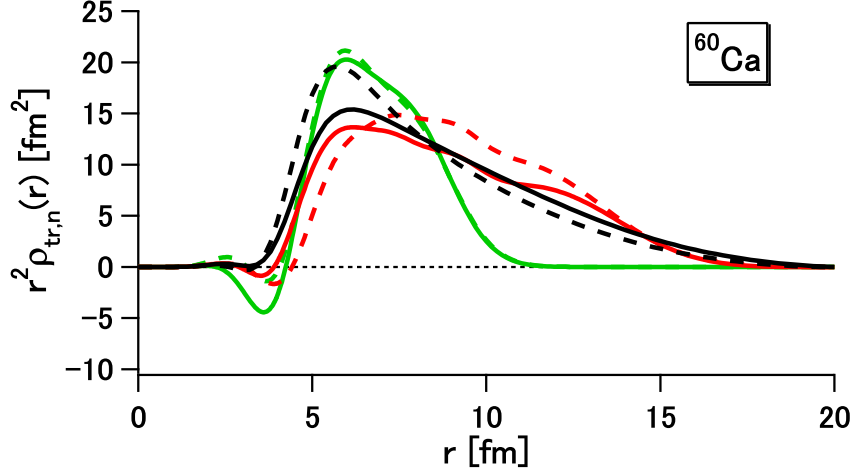


Figure 6: $r^2 \rho_{\text{tr},n}^{(\lambda=3)}(r; \alpha)$ for low-energy states α in ^{60}Ca . The red solid (dashed) line is obtained by the GEM at $\omega_\alpha = 5.02$ MeV (6.68 MeV), while the green solid (dashed) line by the quasi-HO basis functions at $\omega_\alpha = 5.11$ MeV (7.37 MeV). All these states carry relatively strong transition strengths of $B_\alpha^{(\lambda=3, \tau=1)} > 5 \times 10^3 \text{ fm}^6$. The black solid (dashed) line is the continuum RPA result at $\omega = 5.02$ MeV (6.92 MeV).

In the next section we shall apply the present method to self-consistent RPA calculations with a finite-range interaction.

4 Application of GEM to self-consistent RPA

The numerical method based on the GEM is applied to self-consistent RPA calculations. We consider the effective nuclear Hamiltonian comprised of the kinetic energy and the effective NN interaction,

$$H_N = K + V_N; \quad K = \sum_i \frac{\mathbf{p}_i^2}{2M}, \quad V_N = \sum_{i<j} v_{ij}. \quad (16)$$

Here i and j are indices of the constituent nucleons. The full Hamiltonian is given by $H = H_N + V_C - H_{\text{c.m.}}$, where V_C stands for the Coulomb interaction among protons and $H_{\text{c.m.}}$ is the c.m. Hamiltonian. We use the A -independent GEM basis functions of Eq. (8) for all the calculations in this section. Once we compute and store the two-body matrix elements of V_N , we can use them both for the MF and the RPA calculations (except the density-dependent part of V_N). The exchange term of V_C is exactly treated [3]. It should be commented that $H_{\text{c.m.}}$ is highly non-local, and therefore is not easy to be handled in the coordinate representation. In contrast, we can easily take into account both the one- and two-body terms of $H_{\text{c.m.}}$ in the GEM.

In the calculations shown below, we adopt the D1S parameter-set [24] of the Gogny interaction [25] for V_N , in which the central channel has finite ranges, and take $^{40,48,60}\text{Ca}$

Table 4: ω_s^2 values (MeV^2) in the self-consistent RPA calculation by the GEM with the D1S interaction.

nuclide	ω_s^2
^{40}Ca	-5.80×10^{-6}
^{48}Ca	-8.61×10^{-6}
^{60}Ca	-2.67×10^{-6}

as examples. Note that ^{60}Ca is located near the neutron drip line in the prediction with D1S [8]. We carry out the RPA calculations on top of the spherical HF solutions for these nuclei.

In Ref. [26], the D1S interaction was applied to the quasiparticle RPA calculations for the Si and Mg nuclei near the β -stability line, by employing the HO basis functions. The present method based on the GEM will be useful for extending such approaches to drip-line nuclei.

4.1 Spurious c.m. motion

It is proved that the spurious states, which are the Nambu-Goldstone modes emerging from the spontaneous symmetry breaking, have zero excitation energy and are separated from the other states in the self-consistent RPA [10]. A typical example is the spurious c.m. motion. However, we do not necessarily have a zero-energy state in practical calculations even if the Hamiltonian keeps the translational invariance, because of finite size of the s.p. space. Conversely, the energy of the spurious c.m. state provides a measure of accuracy of the numerical calculation.

We here express the lowest 1^- state in the solution of the RPA equation, which corresponds to the spurious c.m. motion, by $\alpha = s$. In Table 4, ω_s^2 values obtained by the GEM basis-set of Eq. (8) are shown for $^{40,48,60}\text{Ca}$. By the GEM the spurious state has zero energy to good precision. Moreover, if the spurious state is well separated, the transition strength $B_\alpha^{(\lambda=1,\tau=0)}$ should vanish for $\alpha \neq s$. We confirm $B_\alpha^{(\lambda=1,\tau=0)} < 10^{-3} \text{ fm}^2$ for all $\alpha (\neq s)$, in any of the three nuclei.

4.2 Energy-weighted sum rules

The RPA preserves the energy-weighted sum rule (EWSR),

$$\Sigma_1 = \sum_\alpha \omega_\alpha \left| \langle \alpha | \mathcal{O} | 0 \rangle \right|^2 = \frac{1}{2} \langle 0 | [\mathcal{O}^\dagger, [H, \mathcal{O}]] | 0 \rangle, \quad (17)$$

if the expectation value of the double commutator is evaluated for the MF ground state [10]. In correspondence to the specific mode $\mathcal{O}^{(\lambda,\tau)}$, we define $\Sigma_1^{(\lambda,\tau)}$. The energy-weighted sum $\Sigma_1^{(\lambda,\tau)}$ is associated with the quantities in Eq. (14) by $\Sigma_1^{(\lambda,\tau)} = \bar{\omega}_D^{(\lambda,\tau)} \cdot B_D^{(\lambda,\tau)}$, for D covering the whole range of ω (*i.e.* $\omega_D^{\min} = 0$ and $\omega_D^{\max} = \infty$). In evaluating

the double commutator, we first take $H' = H_N + V_C$, ignoring $H_{\text{c.m.}}$, instead of the full Hamiltonian H . Most effective interactions (or energy density functionals) including the Skyrme, the Gogny and the M3Y-type ones [7, 8] lead to the continuity equation for the isoscalar density and current (as long as we use H'), from which the following EWSR for the isoscalar transition is derived [27],

$$\begin{aligned}\Sigma_1'^{(\lambda, \tau=0)} &= \frac{1}{2} \langle 0 | [\mathcal{O}^{(\lambda, \tau=0)\dagger}, [H', \mathcal{O}^{(\lambda, \tau=0)}]] | 0 \rangle \\ &= \frac{1}{2} \langle 0 | [\mathcal{O}^{(\lambda, \tau=0)\dagger}, [K, \mathcal{O}^{(\lambda, \tau=0)}]] | 0 \rangle = \frac{\lambda(2\lambda+1)^2}{4\pi} \frac{1}{2M} \langle 0 | \sum_i r_i^{2\lambda-2} | 0 \rangle, \quad (18)\end{aligned}$$

where we restrict ourselves to $\lambda \geq 2$. Though not written explicitly, the z -components of $\mathcal{O}^{(\lambda, \tau)}$ are summed up. However, $H_{\text{c.m.}}$ modifies the EWSR as

$$\begin{aligned}\Sigma_1^{(\lambda, \tau=0)} &= \frac{1}{2} \langle 0 | [\mathcal{O}^{(\lambda, \tau=0)\dagger}, [H, \mathcal{O}^{(\lambda, \tau=0)}]] | 0 \rangle \\ &= \frac{\lambda(2\lambda+1)^2}{4\pi} \frac{1}{2M} \left[\langle 0 | \sum_i r_i^{2\lambda-2} | 0 \rangle \right. \\ &\quad \left. - \frac{4\pi}{2\lambda-1} \frac{1}{A} \langle 0 | \left(\sum_i r_i^{\lambda-1} Y^{(\lambda-1)}(\hat{\mathbf{r}}_i) \right) \cdot \left(\sum_i r_i^{\lambda-1} Y^{(\lambda-1)}(\hat{\mathbf{r}}_i) \right) | 0 \rangle \right] \\ &= \frac{\lambda(2\lambda+1)^2}{4\pi} \frac{1}{2M} \left[\left(1 - \frac{1}{A} \right) \langle 0 | \sum_i r_i^{2\lambda-2} | 0 \rangle \right. \\ &\quad \left. - \frac{4\pi}{2\lambda-1} \frac{1}{A} \langle 0 | \sum_{i \neq j} r_i^{\lambda-1} Y^{(\lambda-1)}(\hat{\mathbf{r}}_i) \cdot r_j^{\lambda-1} Y^{(\lambda-1)}(\hat{\mathbf{r}}_j) | 0 \rangle \right]. \quad (19)\end{aligned}$$

For the $\lambda = 2$ case, Eq. (19) can be rewritten as

$$\Sigma_1^{(\lambda=2, \tau=0)} = \frac{50}{4\pi} \frac{1}{2M} \langle 0 | \sum_i (\mathbf{r}_i - \mathbf{R})^2 | 0 \rangle, \quad (20)$$

where \mathbf{R} denotes the c.m. position. This correction due to $H_{\text{c.m.}}$ is harmonious with the c.m. correction to the rms matter radius [7]. The EWSR of Eq. (19) can be used as another tool to check appropriateness of the s.p. space adopted in the numerical calculation.

For the $(\lambda = 1, \tau = 1)$ mode, the Thomas-Reich-Kuhn (TRK) sum rule is derived if V_N is local,

$$\Sigma_{\text{TRK}} = \frac{1}{2} \langle 0 | [\tilde{\mathcal{O}}^{(\lambda=1, \tau=1)\dagger}, [K, \tilde{\mathcal{O}}^{(\lambda=1, \tau=1)}]] | 0 \rangle = \frac{9}{4\pi} \frac{1}{2M} \frac{4ZN}{A}. \quad (21)$$

However, $\Sigma_1^{(\lambda=1, \tau=1)}$ shifts from Σ_{TRK} in practice, owing to the non-locality in the charge exchange term of V_N . The enhancement factor κ is defined by

$$\Sigma_1^{(\lambda=1, \tau=1)} = (1 + \kappa) \Sigma_{\text{TRK}}. \quad (22)$$

It is noted that $H_{\text{c.m.}}$ does not influence the energy-weighted sum of the $(\lambda = 1, \tau = 1)$ mode (*i.e.* $[\tilde{O}^{(\lambda=1, \tau=1)\dagger}, [H_{\text{c.m.}}, \tilde{O}^{(\lambda=1, \tau=1)}]] = 0$), as long as it is fully taken into account. The enhancement factor κ can be expressed by an expectation value of the charge exchange term of V_N for the ground state. In the case of the Skyrme interaction, an explicit expression of κ in terms of the neutron and proton densities has been given in Ref. [28]. It is complicated to evaluate κ in an individual nucleus if V_N is taken to be a finite-range interaction. However, κ in the symmetric nuclear matter is related to the Landau-Migdal parameter f'_1 [7] by

$$1 + \kappa = \frac{M}{M^*} \left(1 + \frac{f'_1}{3}\right), \quad (23)$$

where M^* denotes the effective k -mass. Equation (23) gives an approximate value of κ for finite nuclei.

In many calculations using the Skyrme interaction, only the one-body term of $H_{\text{c.m.}}$ is taken into account. We point out that this prescription influences the above sum rules. For the $(\lambda \geq 2, \tau = 0)$ modes, the energy-weighted sum becomes $\Sigma_1^{(\lambda, \tau=0)}$ multiplied by $(1 - 1/A)$, lacking the second term in the last expression of Eq. (19). Moreover, if we subtract only the one-body term of $H_{\text{c.m.}}$, the TRK part of the energy-weighted sum for the $(\lambda = 1, \tau = 1)$ mode (*i.e.* Eq. (21)) is fictitiously reduced by $(1 - 1/A)$.

As an indicator for the EWSR, we define the ratio,

$$\mathcal{R}^{(\lambda, \tau)} = \sum_{\alpha} \omega_{\alpha} \left| \langle \alpha | \mathcal{O}^{(\lambda, \tau)} | 0 \rangle \right|^2 / \frac{1}{2} \langle 0 | [\mathcal{O}^{(\lambda, \tau)\dagger}, [H, \mathcal{O}^{(\lambda, \tau)}]] | 0 \rangle, \quad (24)$$

which should be unity if the s.p. basis-set is complete. In Table 5, we show $\mathcal{R}^{(\lambda, \tau=0)}$ ($\lambda = 2, 3$) in $^{40,48,60}\text{Ca}$. It is confirmed that the present method satisfies the EWSRs of Eq. (19) within a few percent precision. For the $(\lambda = 1, \tau = 1)$ mode, we use the ratio to the TRK sum rule,

$$\tilde{\mathcal{R}}_K^{(\lambda=1, \tau=1)} = \sum_{\alpha} \omega_{\alpha} \left| \langle \alpha | \tilde{\mathcal{O}}^{(\lambda=1, \tau=1)} | 0 \rangle \right|^2 / \frac{1}{2} \langle 0 | [\tilde{\mathcal{O}}^{(\lambda=1, \tau=1)\dagger}, [K, \tilde{\mathcal{O}}^{(\lambda=1, \tau=1)}]] | 0 \rangle, \quad (25)$$

and compare it with the rhs of Eq. (23), which is denoted by $\tilde{\mathcal{R}}_{K, \infty}^{(\lambda=1, \tau=1)}$. The values of $\tilde{\mathcal{R}}_K^{(\lambda=1, \tau=1)}$ ($= 1 + \kappa$) are presented in Table 6. The $\tilde{\mathcal{R}}_K^{(\lambda=1, \tau=1)}$ value does not depend strongly on nuclides. The nuclear matter value of $\tilde{\mathcal{R}}_{K, \infty}^{(\lambda=1, \tau=1)}$ gives a good first approximation, and slight reduction from $\tilde{\mathcal{R}}_{K, \infty}^{(\lambda=1, \tau=1)}$ may be accounted for mainly by the difference between $\rho_p(\mathbf{r})$ and $\rho_n(\mathbf{r})$ [28]. It is noted that the experimental value has been reported as $\tilde{\mathcal{R}}_K^{(\lambda=1, \tau=1)} = 1.76 \pm 0.10$ [29], being almost independent of the mass number.

4.3 Strength functions

We next show the strength functions $S_{\gamma}^{(\lambda, \tau)}(\omega)$ obtained by the self-consistent RPA calculations with D1S, in Figs. 7–11. We here adopt $\gamma = 0.4 \text{ MeV}$. The strength functions in the RPA are compared with the unperturbed strength functions, in which the residual interaction is ignored.

Table 5: $\mathcal{R}^{(\lambda,\tau=0)}$ in the RPA calculation by the GEM, in which the D1S interaction is employed.

nuclide	λ	$\mathcal{R}^{(\lambda,\tau=0)}$
^{40}Ca	2	1.005
	3	1.031
^{48}Ca	2	1.006
	3	1.033
^{60}Ca	2	1.003
	3	1.010

Table 6: $\tilde{\mathcal{R}}_K^{(\lambda=1,\tau=1)}$ in the RPA calculation by the GEM, in comparison with the nuclear matter value $\tilde{\mathcal{R}}_{K,\infty}^{(\lambda=1,\tau=1)} = (M/M^*) (1 + f'_1/3)$. The D1S interaction is used.

nuclide	$\tilde{\mathcal{R}}_K^{(\lambda=1,\tau=1)}$	$\tilde{\mathcal{R}}_{K,\infty}^{(\lambda=1,\tau=1)}$
^{40}Ca	1.587	
^{48}Ca	1.589	1.660
^{60}Ca	1.584	

Irrespectively of (λ, τ) , the strength functions $S_\gamma^{(\lambda,\tau)}(\omega)$ with the D1S force are qualitatively similar to those obtained with the schematic interaction shown in Sec. 3. Significant difference between the RPA strength function and the unperturbed one suggests collectivity of the transition. In this regard we view collectivity of the isovector giant dipole resonance (IV-GDR) induced by a repulsive part of the residual interaction in Fig. 7, and of the isoscalar giant quadrupole and octupole resonances (IS-GQR and IS-GOR) induced by an attractive interaction in Figs. 8 and 10. Collectivity of these giant resonances is further confirmed from the forward and backward amplitudes of the state that forms the highest peak in the strength function; a number of the unperturbed excitations are mixed in the RPA states.

In ^{60}Ca , transition strengths emerge and form a peak in $S_\gamma^{(\lambda,\tau)}$ at relatively low energy ($\omega \lesssim 10$ MeV), though the transitions are not so strong as in the giant resonances. It is of interest whether such low-energy strengths have collective nature or not. By comparing the RPA strength functions to the unperturbed ones, it is suggested that the low-energy transitions specific to ^{60}Ca hardly have strong collectivity. This consequence is consistent with the argument in Ref. [30], and will further be investigated in a forthcoming paper. For the $(\lambda = 1, \tau = 1)$ mode, the low-energy strengths may be compared to the so-called pygmy dipole resonance (PDR) that has been observed in several $Z < N$ nuclei such as ^{90}Zr [31] and ^{208}Pb [32]. The IV-GDR in $Z \sim N$ nuclei is interpreted as a surface oscillation to which the protons and the neutrons contribute with opposite phases. In the neutron-rich nuclei the $E1$ transition could have two collective components; an oscillation

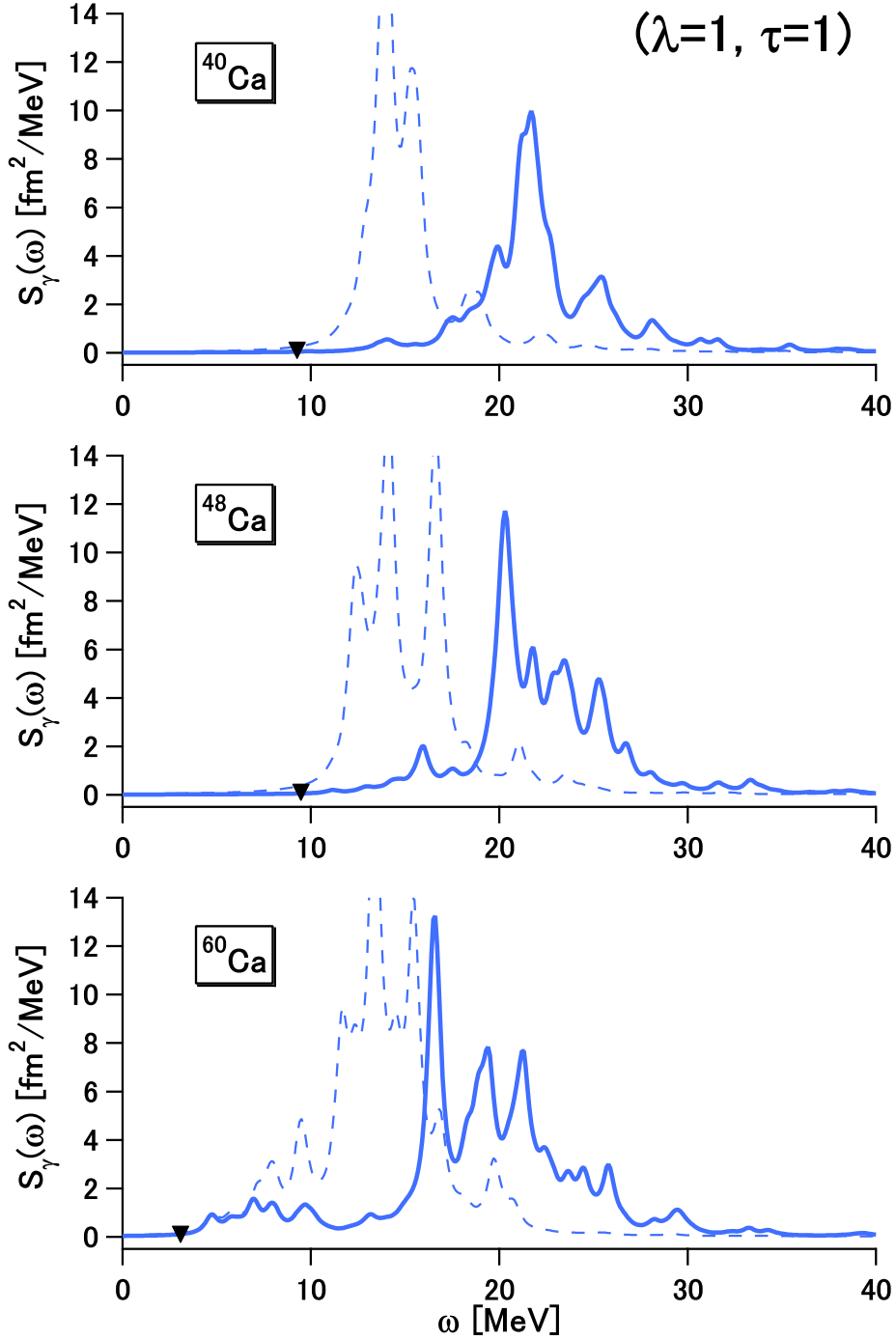


Figure 7: $\tilde{S}_\gamma^{(\lambda=1, \tau=1)}(\omega)$ in $^{40,48,60}\text{Ca}$. We take $\gamma = 0.4 \text{ MeV}$. The solid lines are obtained by the self-consistent RPA calculations with the D1S interaction, while the dashed lines represent the unperturbed strength functions. The particle threshold energy in the HF approximation is indicated by the inverted triangle for each nucleus.

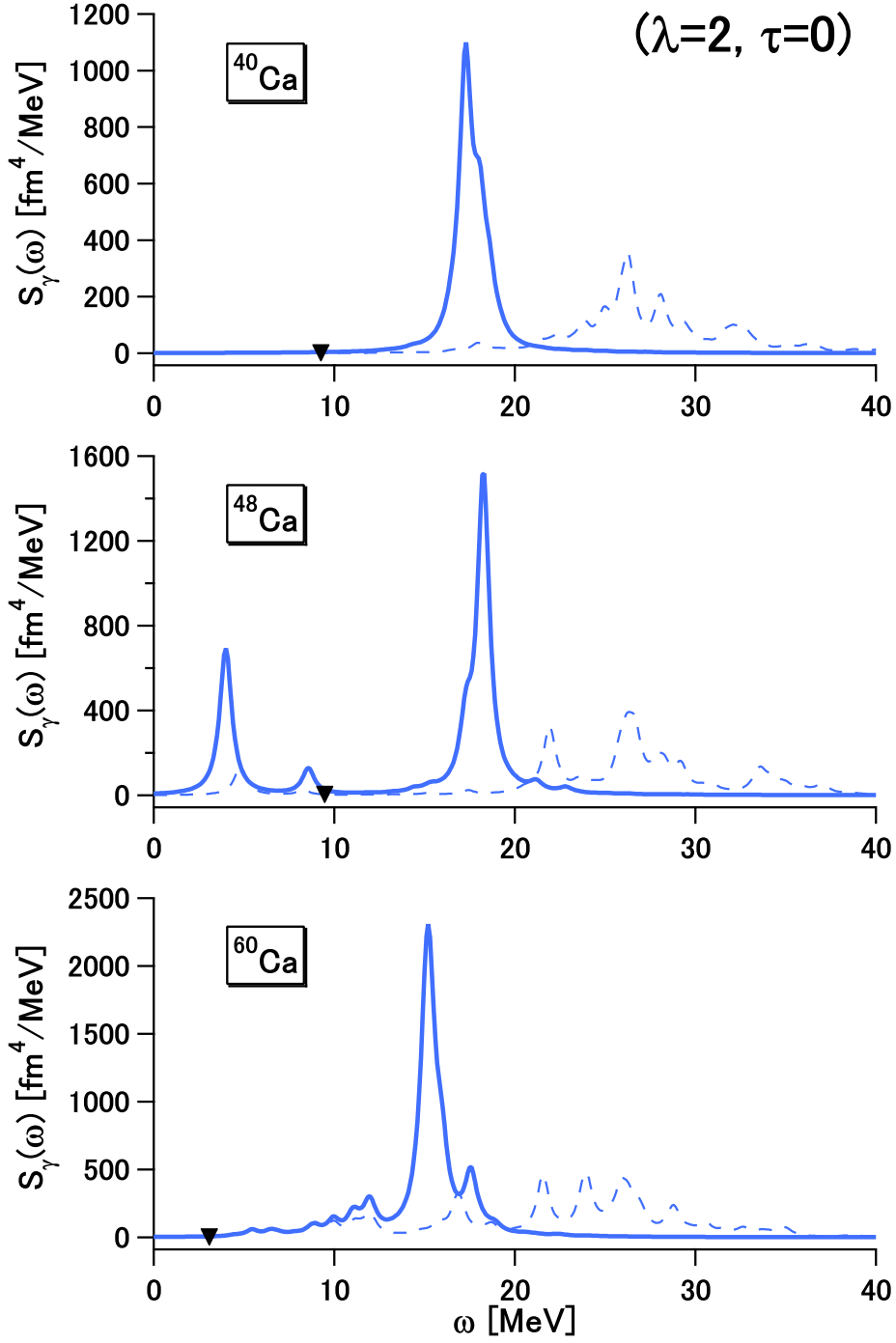


Figure 8: $S_\gamma^{(\lambda=2, \tau=0)}(\omega)$ in $^{40,48,60}\text{Ca}$ calculated with the D1S interaction. Conventions are the same as in Fig. 7.

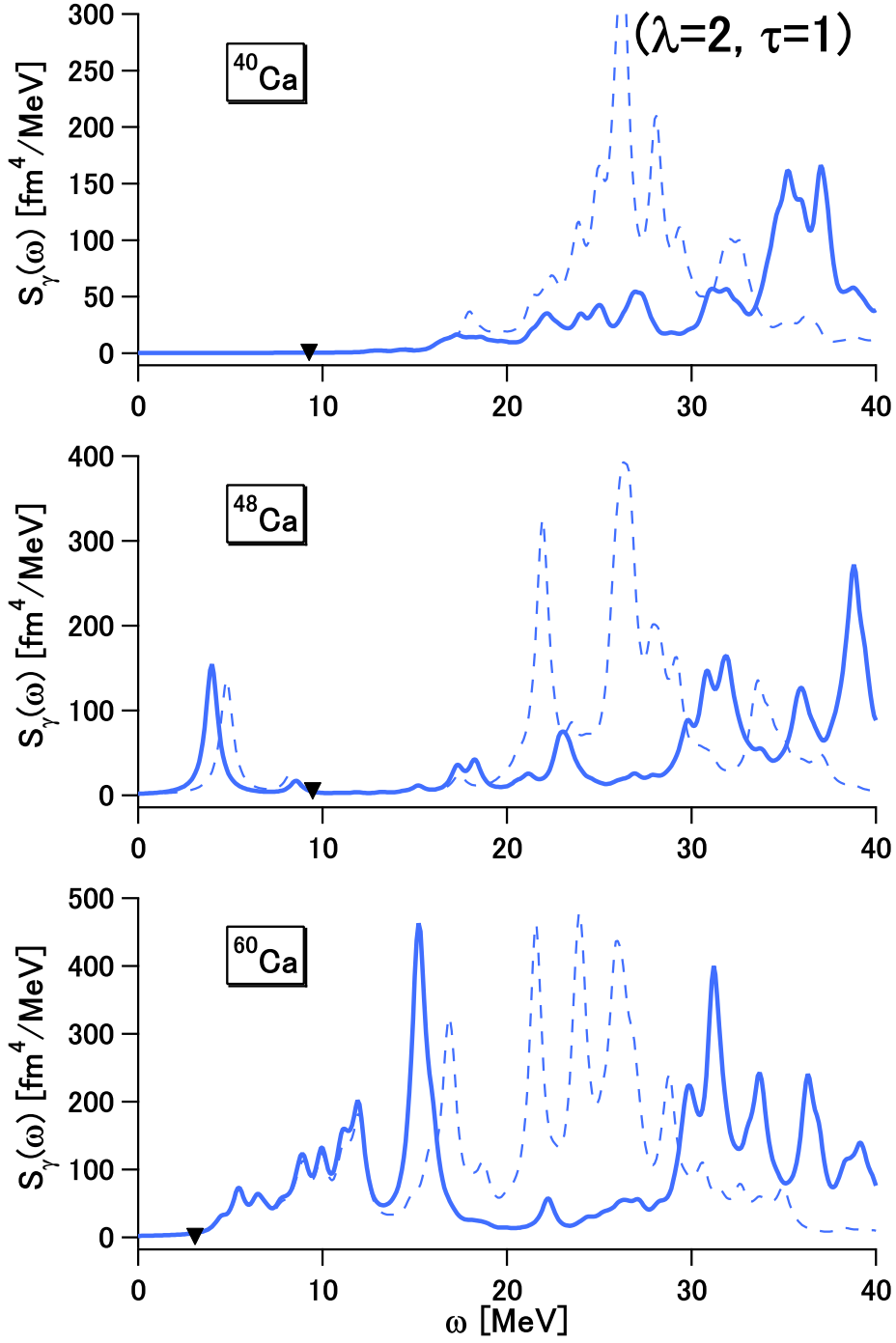


Figure 9: $S_{\gamma}^{(\lambda=2, \tau=1)}(\omega)$ in $^{40,48,60}\text{Ca}$ calculated with the D1S interaction. Conventions are the same as in Fig. 7.

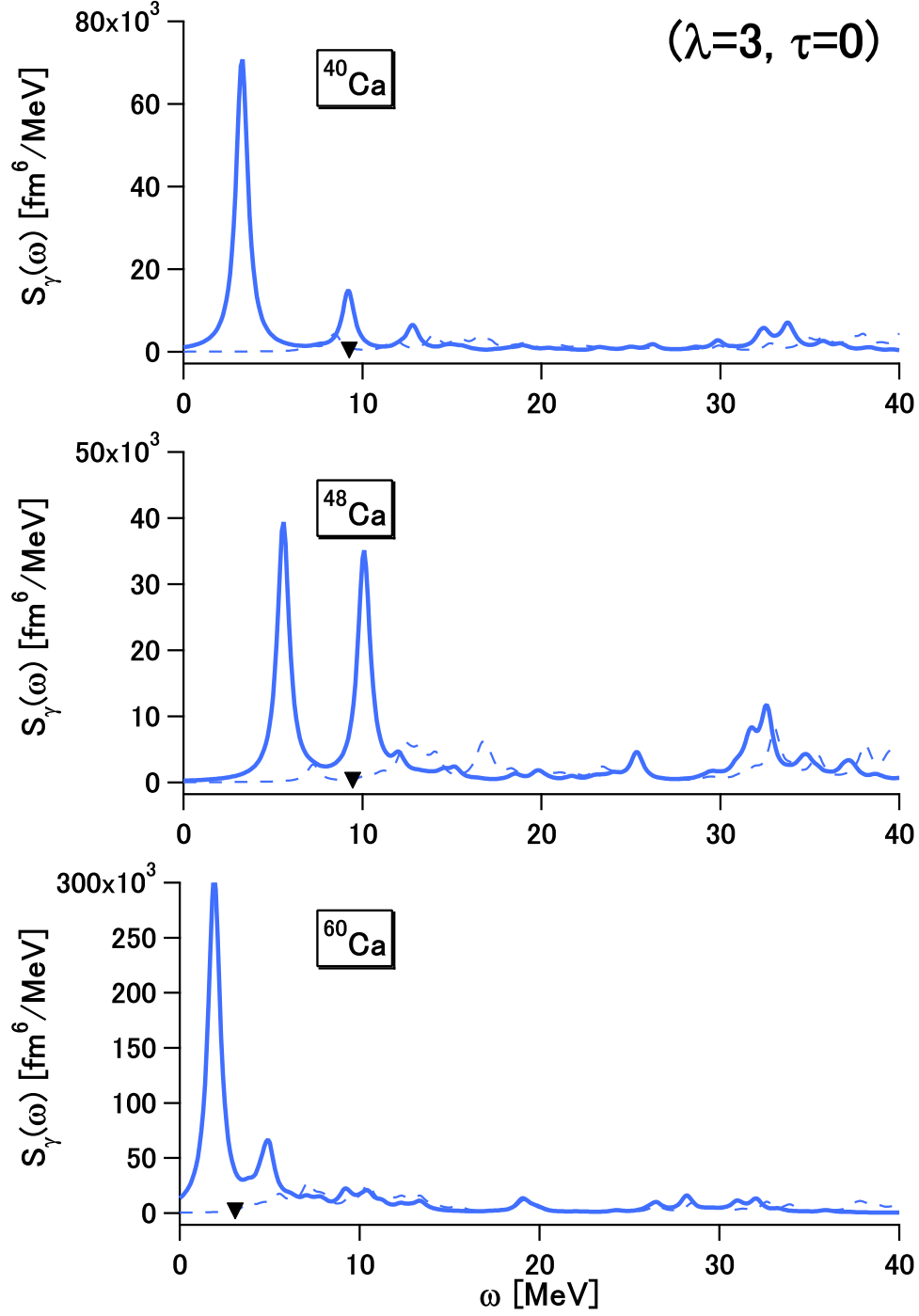


Figure 10: $S_\gamma^{(\lambda=3, \tau=0)}(\omega)$ in $^{40,48,60}\text{Ca}$ calculated with the D1S interaction. Conventions are the same as in Fig. 7.

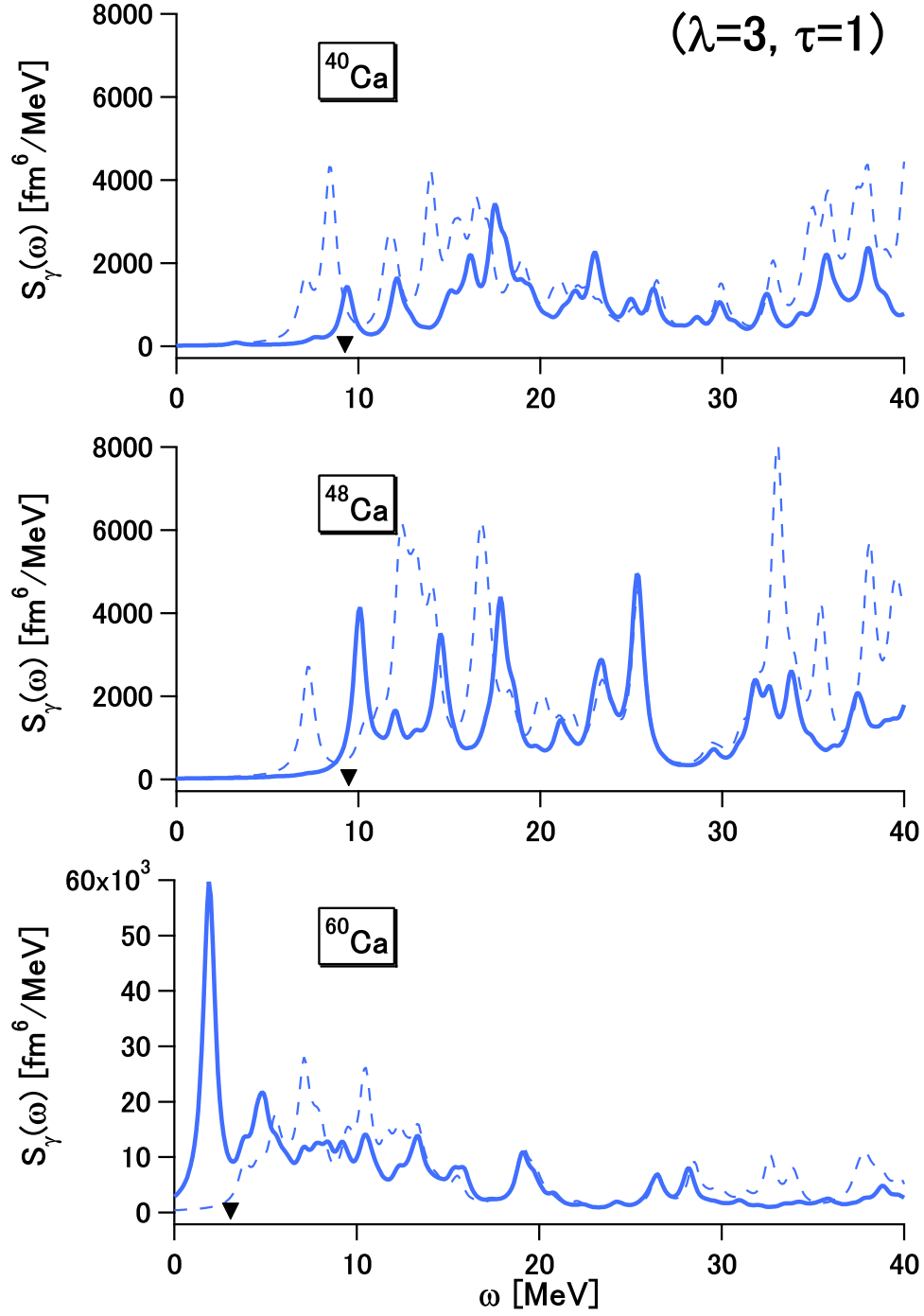


Figure 11: $S_\gamma^{(\lambda=3, \tau=1)}(\omega)$ in $^{40,48,60}\text{Ca}$ calculated with the D1S interaction. Conventions are the same as in Fig. 7.

between protons and neutrons, and an oscillation between a core and excess neutrons. The latter is a possible interpretation of the PDR. In Fig. 12 the neutron and proton transition densities in ^{60}Ca are depicted for the $\omega_\alpha = 6.9$ MeV and 16.5 MeV states, both of which form the peaks in Fig. 7. We here define the transition density by

$$r^2 \tilde{\rho}_{\text{tr},\tau_z}^{(\lambda=1)}(r; \alpha) = \begin{cases} \frac{2Z}{A} \langle \alpha | \sum_{i \in n} \delta(r - r_i) r_i Y^{(1)}(\hat{\mathbf{r}}_i) | 0 \rangle & (\text{for } \tau_z = n) \\ \frac{2N}{A} \langle \alpha | \sum_{i \in p} \delta(r - r_i) r_i Y^{(1)}(\hat{\mathbf{r}}_i) | 0 \rangle & (\text{for } \tau_z = p) \end{cases}, \quad (26)$$

which is analogous to Eq. (15) but is subject to the modification of Eq. (12). Because the spurious c.m. motion is well separated, we have

$$\int dr \cdot r^2 \rho_{\text{tr,IS}}^{(\lambda=1)}(r; \alpha) = 0, \quad (27)$$

where the isoscalar transition density is defined by

$$r^2 \rho_{\text{tr,IS}}^{(\lambda=1)}(r; \alpha) = \frac{A}{2NZ} [N \cdot r^2 \tilde{\rho}_{\text{tr},n}^{(\lambda=1)}(r; \alpha) + Z \cdot r^2 \tilde{\rho}_{\text{tr},p}^{(\lambda=1)}(r; \alpha)]. \quad (28)$$

Figure 12 shows that, to the first approximation, the higher-lying strength corresponds to an out-of-phase oscillation between protons and neutrons as in the usual IV-GDR, while the lower-lying strength looks like an oscillation between a core and outer neutrons, as pointed out in Ref. [33]. It should be noted that the peaks in $r^2 \tilde{\rho}_{\text{tr},\tau_z}^{(\lambda=1)}(r; \alpha)$ are considerably displaced between $\tau_z = n$ and p for the transition to the $\omega_\alpha = 16.5$ MeV state. This indicates that, whereas $r^2 \rho_{\text{tr,IS}}^{(\lambda=1)}(r; \alpha)$ is vanishingly small in the $Z \sim N$ nuclei such as ^{40}Ca , it does not vanish in ^{60}Ca even for the strong transition, though satisfying Eq. (27). Moreover, behavior of $r^2 \tilde{\rho}_{\text{tr},n}^{(\lambda=1)}(r; \alpha)$ at $r \approx 4$ fm suggests that this state contains a weak admixture of the oscillation between a core and outer neutrons.

5 Summary

We have developed a method of implementing RPA calculations, which is based on the Gaussian expansion method (GEM). Owing to the advantages of the GEM which have been established in the MF calculations, it is naturally expected that we can efficiently compute excitation of nuclei including coupling to the continuum. The parameters of the s.p. basis functions are insensitive to nuclide, and even calculations with a single set of bases may cover wide range of the mass table.

The method has first been tested in $^{40,48,60}\text{Ca}$ with a density-dependent contact interaction on top of the Woods-Saxon single-particle (s.p.) states, by comparing its results with the results obtained with the continuum RPA method. We have confirmed that the present method using the GEM basis functions of Eq. (8) describes the energies, the transition strengths and the widths of their distribution with good precision for the 1^- , 2^+ and 3^- collective states, including drip-line nuclei, although we cannot reproduce the

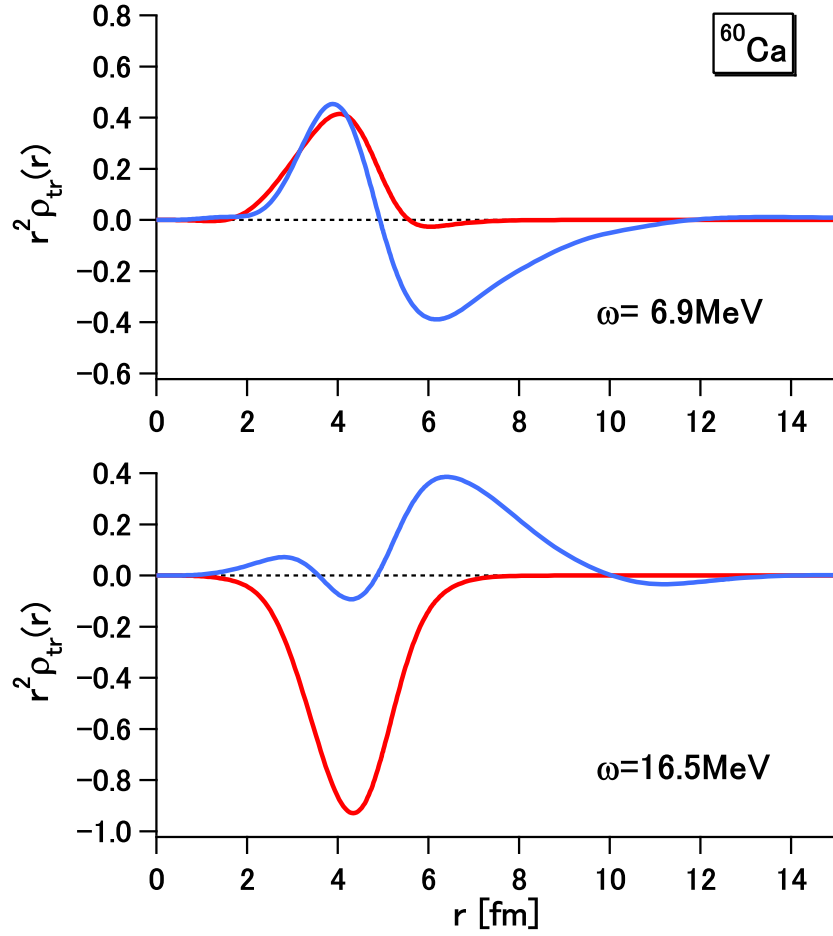


Figure 12: $r^2 \tilde{\rho}_{\text{tr}, \tau_z}^{(\lambda=1)}(r; \alpha)$ in ^{60}Ca for the $\omega_\alpha = 6.9$ and 16.5 MeV states, obtained by the RPA calculation with the D1S interaction. The blue (red) line is for $\tau_z = n$ (p).

smooth energy dependence of the transition strengths in the continuum. The new method has been compared also with the box-boundary method and with the method using bases analogous to the harmonic-oscillator (HO) ones. The present method attains precision comparable to the box-boundary method of $r_{\text{max}} = 20$ fm. The basis-set similar to the HO set of $N_{\text{osc}} \leq 11$ does not give good precision, particularly for low-energy transitions in drip-line nuclei, because it is unable to reproduce transition densities at $r \gtrsim 10$ fm. It may not be easy to describe such transitions appropriately even if we take a larger number of the HO basis functions.

Another advantage of the present method is its tractability of finite-range interactions. This point has been demonstrated by the application to the self-consistent HF plus RPA calculations in $^{40,48,60}\text{Ca}$ with the Gogny D1S interaction. It has been confirmed that the zero excitation energy of the spurious state and the energy-weighted sum rules for the isoscalar transitions are fulfilled to good precision. By comparing the RPA strength functions to the unperturbed ones, collectivity of the transitions has been argued. For ^{60}Ca , characters of the low-energy dipole strengths have been investigated as well as those of the giant dipole resonance, via the transition densities.

Further application of the present method to excitations of nuclei with finite-range interactions, including the semi-realistic interactions [7, 8], is under progress. We here mention a study of the $M1$ transition in ^{208}Pb [34], in which significant effects of the tensor force have been confirmed. Future plans include extension of the present method to the quasiparticle RPA, which is quite promising since the GEM has been successfully applied to the Hartree-Fock-Bogolyubov calculations [4].

The authors are grateful to T. Nakatsukasa for discussions. This work is financially supported in part as Grant-in-Aid for Scientific Research (C), No. 19540262, by Japan Society for the Promotion of Science. Numerical calculations were performed on HITAC SR11000 at Institute of Media and Information Technology, Chiba University, on HITAC SR11000 at Information Initiative Center, Hokkaido University, and on NEC SX-8 at Yukawa Institute for Theoretical Physics, Kyoto University.

References

- [1] I. Tanihata, Prog. Part. Nucl. Phys. **35** (1995) 505.
- [2] A. Ozawa, T. Kobayashi, T. Suzuki, K. Yoshida and I. Tanihata, Phys. Rev. Lett. **84** (2000) 5493 R. Kanungo, I. Tanihata and A. Ozawa, Phys. Lett. B **528** (2002) 58.
- [3] H. Nakada and M. Sato, Nucl. Phys. **A699** (2002) 511; *ibid.* **A714** (2003) 696.
- [4] H. Nakada, Nucl. Phys. **A764** (2006) 117; *ibid.* **A801** (2008) 169.
- [5] H. Nakada, Nucl. Phys. **A808** (2008) 47.

- [6] E. Hiyama, Y. Kino and M. Kamimura, *Prog. Part. Nucl. Phys.* **51** (2003) 223.
- [7] H. Nakada, *Phys. Rev. C* **68** (2003) 014316.
- [8] H. Nakada, *Phys. Rev. C* **78** (2008) 054301.
- [9] S. Shlomo and G. Bertsch, *Nucl. Phys.* **A243** (1975) 507.
- [10] P. Ring and P. Schuck, *The Nuclear Many-Body Problem* (Springer-Verlag, New York, 1980).
- [11] G. Giambrone *et al.*, *Nucl. Phys.* **A726** (2003) 3.
- [12] G.F. Bertsch and S.F. Tsai, *Phys. Rep.* **18** (1975) 125.
- [13] M. Matsuo, *Nucl. Phys.* **A696** (2001) 371.
- [14] K. Mizuyama, M. Matsuo and Y. Serizawa, *Phys. Rev. C* **79** (2009) 024313.
- [15] H. Imagawa and Y. Hashimoto, *Phys. Rev. C* **67** (2003) 037302; T. Inakura *et al.*, *Nucl. Phys.* **A768** (2006) 61.
- [16] R.H. Lemmer and M. Vénérone, *Phys. Rev.* **170** (1968) 883.
- [17] T. Nakatsukasa and K. Yabana, *Phys. Rev. C* **71** (2005) 024301.
- [18] T. Nakatsukasa, T. Inakura and K. Yabana, *Phys. Rev. C* **76** (2007) 024318.
- [19] J.P. Blaizot and D. Gogny, *Nucl. Phys.* **A284** (1977) 429.
- [20] M. Matsuo, K. Mizuyama and Y. Serizawa, *Phys. Rev. C* **71** (2005) 064326.
- [21] I. Hamamoto, H. Sagawa and X.Z. Zhang, *Nucl. Phys.* **A626** (1997) 669.
- [22] I. Hamamoto, H. Sagawa and X.Z. Zhang, *Phys. Rev. C* **64** (2001) 024313.
- [23] H. Sagawa, *Prog. Theor. Phys. Suppl.* **142** (2001) 1.
- [24] J.F. Berger, M. Girod and D. Gogny, *Comp. Phys. Comm.* **63** (1991) 365.
- [25] J. Dechargé and D. Gogny, *Phys. Rev. C* **21** (1980) 1568.
- [26] S. Péru and H. Goutte, *Phys. Rev. C* **77** (2008) 044313.
- [27] T. Suzuki, *Prog. Theor. Phys.* **64** (1980) 1627.
- [28] T. Sil, S. Shlomo, B.K. Agrawal and P.-G. Reinhardt, *Phys. Rev. C* **73** (2006) 034316.
- [29] A. Leprêtre *et al.*, *Nucl. Phys.* **A367** (1981) 237.
- [30] F. Catara, C.H. Dasso and A. Vitturi, *Nucl. Phys.* **A602** (1996) 181.

- [31] R. Schwengner *et al.*, Phys. Rev. C **78** (2008) 064314.
- [32] R.D. Starr, P. Axel and L.S. Cardman, Phys. Rev. C **25** (1982) 780; Z.W. Bell, L.S. Cardman and P. Axel, Phys. Rev. C **25** (1982) 791; G. Kühner *et al.*, Phys. Lett. **B104** (1981) 189.
- [33] J. Terasaki and J. Engel, Phys. Rev. C **74** (2006) 044301.
- [34] T. Shizuma *et al.*, Phys. Rev. C **78** (2008) 061303.